www.sciencemag.org/cgi/content/full/science.1260088/DC1

Supplementary Material for

Expansion Microscopy

Fei Chen, Paul W. Tillberg, Edward S. Boyden*

*Corresponding author. E-mail: esb@media.mit.edu

Published 15 January 2015 on *Science* Express
DOI: 10.1126/science.1260088

This PDF file includes:

Other Supplementary Material for this manuscript includes the following:
(available at www.sciencemag.org/content/science.1260088/DC1)

Science
AAAS

Supplementary Materials:

Materials and Methods

A complete list of chemicals and supplier catalog numbers used can be found in **Table S2**.

Labels for ExM: DNA sequences on secondary antibodies were synthesized with 5' amine modification (Integrated DNA Technologies) and conjugated to the antibodies (Jackson ImmunoResearch, Affinipure donkey antibodies) using a commercial kit (Solulink, Antibody-Oligonucleotide All-in-One Conjugation Kit). For the tri-functional label, the oligonucleotides were synthesized with a 3' amine modification and a 5' Acrydite modification (Integrated DNA Technologies), then conjugated to dyes (Alexa 488, Atto 565 and Atto 647N) modified with NHS-ester chemistry per the dye manufacturer's directions (see **Table S3** for sequences). We found that Cy5 undergoes strong bleaching during polymerization, most likely due to the radical reactivity of its simple linear conjugated backbone, while other fluorophores tested retained at least 50% of their brightness (**Table S1**). Tri-functional labels were purified via reverse-phase HPLC, lyophilized, and re-suspended in ddH_2O.

Cultured cell preparation and staining: HEK293-FT cells (Invitrogen) were cultured in Culturewell Chambered Coverglasses (Invitrogen) per manufacturer's instructions. All solutions below were made up in 1x phosphate buffered saline (PBS), and incubations carried out at room temperature. To preserve microtubule ultrastructure, cells were fixed, as in (*6*), in 3% formaldehyde/0.1% glutaraldehyde for 10 minutes, followed by reduction with 0.1% $NaBH_4$ for 7 minutes, and quenching in 100 mM glycine for 10 minutes. For clathrin, cells were fixed in 4% formaldehyde for 10 minutes followed by quenching in 100 mM glycine for 10 minutes. Cells were permeabilized with 0.2% Triton X-100 for 15 minutes at room temperature and blocked with 5% normal donkey serum for one hour. Specimens were incubated with primary antibodies (Sheep anti-Tubulin, Cytoskeleton ATN02; Rabbit anti-Clathrin, Abcam AB21679) in blocking buffer at a concentration of 10 μg/mL for 1-4 hours, and then washed in PBS three times for 5 minutes each. Specimens were incubated with DNA-labeled secondary antibodies in DNA hybridization buffer (2x saline-sodium citrate (SSC) buffer, 10% dextran sulfate, 1 mg/mL yeast tRNA, 5% normal donkey serum) at a concentration of approximately 10 μg/mL for 1-4 hours, then washed in PBS as for primary. Specimens were incubated with tri-functional labels in hybridization buffer at a concentration of 0.5 ng/μL for each oligonucleotide overnight, then washed three times in 1x PBS.

Brain tissue preparation and staining: All procedures involving animals were in accordance with the US National Institutes of Health Guide for the Care and Use of Laboratory Animals and approved by the Massachusetts Institute of Technology Committee on Animal Care. All solutions below were made up in 1x phosphate buffered saline (PBS), and incubations carried out at room temperature unless otherwise noted. Mice, wildtype (C57BL/6, obtained from Taconic) and transgenic expressing cytosolic YFP under the Thy1 promoter (Thy1-YFP-H strain on C57BL/6, obtained from Jax), were anesthetized with isoflurane and perfused transcardially with ice cold 4% paraformaldehyde. Brains were dissected out, left in 4% paraformaldehyde at 4^oC for one day, and then sunk in 30% sucrose with 100 mM glycine for one day. Slices greater than 30 μm thick were sliced on a vibratome (Leica VT1000S); slices 30 μm thick were frozen in -40^o C isopentane cooled with dry ice, embedded in M-1 embedding matrix (Thermo Scientific) and sliced on a cryotome (Leica CM1850UV). Slices were permeabilized and blocked

with 0.1% Triton X-100 and 2% normal donkey serum (slice blocking buffer) for at least six hours. Slices were incubated with primary antibodies in slice blocking buffer at a concentration of 10 μg/mL for 6-24 hours depending on slice thickness and antibody, and then washed in slice blocking buffer four times, for thirty minutes each time, changing solutions in between. Slices were incubated with DNA-labeled secondary antibodies in hybridization buffer plus 0.1% Triton X-100 at a concentration of approximately 10 μg/mL for 6-24 hours depending on slice thickness and antibody, then washed in slice blocking buffer as for primary. Specimens were incubated with tri-functional labels in hybridization buffer plus 0.1% Triton X-100 at a concentration of 0.5 ng/μL per oligonucleotide for 6-12 hours, then washed in slice blocking buffer as for primary. Slices used were 30 μm (for the bleaching experiments of **Table S1**), 200 μm (**Fig. 1, Fig. S2**), or 100 μm (all other figures with slices) thick.

For **Figs. 3** and **4**, slices were stained with primary antibodies Chicken anti-GFP, Millipore AB16901; Rabbit anti-Homer1, Synaptic Systems 160003; Mouse anti-Bassoon, Abcam AB82958. For **Fig. S4**, antibodies used were Rabbit anti-GAD65/67, Chemicon AB1511; Rabbit anti-ChAT, Millipore AB143; Rabbit anti-CaMKII, Epitomics 2048-1; Rabbit anti-GABA, Sigma A2052; Mouse anti-Lamin A/C, Cell Signaling Technology #4777; Rabbit anti-NMDAR2a/b, Millipore AB1548.

In situ polymer synthesis: Monomer solution (1x PBS, 2 M NaCl, 8.625% (w/w) sodium acrylate, 2.5% (w/w) acrylamide, 0.15% (w/w) N,N'-methylenebisacrylamide) was mixed (see **Table S4**), frozen in aliquots, and thawed before use. Prior to embedding, monomer solution was cooled to 4°C to prevent premature gelation. Concentrated stocks (10% w/w) of ammonium persulfate (APS) initiator and tetramethylethylenediamine (TEMED) accelerator were added to the monomer solution up to 0.2% (w/w) each. For slices, the inhibitor 4-hydroxy-2,2,6,6-tetramethylpiperidin-1-oxyl (4-hydroxy-TEMPO) was added up to 0.01% (w/w) from a 1% (w/w) stock to inhibit gelation during diffusion of the monomer solution into tissue sections. Stained cells or tissue slices were incubated with the monomer solution plus APS/TEMED (and 4-hydroxy-TEMPO for slices) at 4°C for one minute, 30 minutes or 45 minutes for cultured cells, 30 μm/100 μm slices and 200 μm slices respectively. Slices were incubated with at least 100-fold excess volume of monomer solution.

For cells, gels were formed directly in a Culturewell Chambered Coverglass (Invitrogen), with monomer solution plus APS/TEMED added to a depth of about 2mm. For tissue slices, gelation chambers were constructed with two pieces of coverglass separated by spacers placed on either side of the tissue section (for 30 and 100 μm sections, #1 coverglasses were used for spacers and for 200 μm sections, a stack of two # 1 coverglasses was used for each spacer). Slices were not placed into coverglass gelation chambers until the end of the monomer incubation period, to ensure adequate access of the monomer solution to the slice. After incubation in monomer solution (and chamber construction, for slices), specimens were transferred to a humidified 37° C incubator for two hours.

Specimen-free gels of **Fig. S5** were cast with the same recipe as for cultured cells except with a variable amount of cross-linker, in forms constructed from two coverslips separated by a silicone gasket 1 mm thick, with circular holes 5.2 mm in diameter. Gels were expanded as with cultured cells, but without needing digestion. Diameters of expanded gels were measured using Vernier calipers to find the linear expansion factor.

Digestion and expansion: Proteinase K (New England Biolabs) was diluted 1:100 to 8 units/mL in digestion buffer (50 mM Tris (pH 8), 1 mM EDTA, 0.5% Triton X-100, 0.8 M guanidine HCl) and applied directly to gels in at least ten times volume excess. Before adding digestion buffer, the coverglass chamber walls (for cultured cells) or the top coverglass of the gelation chamber (for tissue slices) was carefully removed in order to improve access of enzyme to the embedded cells. The gels were then incubated in digestion buffer for at least 12 hours. Digested gels were next placed in excess volumes of doubly de-ionized water for 0.25-2 hours to expand, with longer times for thicker gels. This step was repeated 3-5 times in fresh water, until the size of the expanding sample plateaued.

Acrydite covalent anchoring efficiency: Label DNA oligonucleotides (A1 and A2, in **Table S3**) were ordered from IDT without the 5' acrydite modification, for the anchoring efficiency experiments of **Table S1**. Specimen-free gels (n = 4 gels) were cast with the same recipe as for cultured cells with addition of DNA labels with and without acrydite modification (0.25 ng/μL of each strand). Following gelation, gels were dialyzed in 20x volume of 10x PBS for 1 day to allow unincorporated DNA labels to equilibrate in concentration with the dialysate. Samples were taken from the dialysate after equilibration and measured on a fluorescence plate reader (Spectramax M5e). A fluorescence standard curve made from serial dilutions of label oligonucleotides was used to determine fluorescence concentration in the dialysate. The incorporation efficiency of non-acrydite labels was confirmed to be zero by fluorescence microscopy of the gels following dialysis equilibration; the ratio of fluorescence intensity inside the gel to the dialysate was 0.99 ± 0.07 (n = 4 samples). Acrydite incorporation efficiency was calculated as 1 – (dialysate concentration with acrydite/dialysate concentration without acrydite).

Chemical bleaching during gelation: Fluorescence intensity in stained brain slices was measured before vs. after expansion for the bleaching experiments of **Table S1**. Wild type brain slices (30 μm thick) containing sections of mouse hippocampus were stained with anti-GABA primary (Sigma A2052) antibody, DNA secondary antibodies, and tertiary DNA bearing either Alexa 488, Atto 565, or Atto 647N as described above. Epifluorescence images of the brain slice were taken with 4x 0.13 NA objective with tiling to cover the entire slice, pre-gelation. Following in situ polymer synthesis as described above, epifluorescence images of the slice were taken again with identical imaging conditions. A region of interest in the hippocampus was used to determine the loss of fluorescence during gelation.

Imaging:

Cultured cells. Super-resolution structured illumination microscope imaging was performed on a Deltavision OMX SIM microscope with 100x 1.40 NA (Olympus) oil objective. Stained cells were imaged with SlowFade Gold (Invitrogen) antifade reagent for suppression of photobleaching and refractive index matching for pre-expansion imaging. Pre-expansion imaging was performed on a Zeiss Laser Scanning Confocal (LSM710) with 40x 1.30 NA oil objective at 1 Airy unit and Nyquist sampling.

Post-expansion imaging was performed on a Perkin Elmer spinning disk (CSU-10 Yokogawa) confocal or a Zeiss LSM 710. Briefly, expanded samples were placed in glass-bottom six-well plates (In Vitro Scientific) and held in place by surrounding with low-melting point agarose. Images were taken at with 1 Airy unit and Nyquist sampling on the LSM 710 on a 20x 0.8 NA (Zeiss) air objective. Images on the Perkin Elmer were taken on a 100x 1.40 NA (Zeiss) oil objective.

Figs. 2A, 2B are maximum intensity projections (MIPs) of 1.5 μm thickness (in pre-ExM distance units). **Figs. 2D, 2E** are MIPs of 1 μm thickness. **Figs. 2K, 2L** are MIPs of 500 nm thickness. The SR-SIM image of **Fig. 2M** is depicted interpolated such that the pixel size is the same as that of the corresponding ExM image of **Fig. 2N**.

Brain slices. To quantify expansion factor for tissue slices, specimens were imaged pre-ExM on a Nikon Ti-E epifluorescence microscope with a 4x 0.13 NA air objective. Otherwise, tissue slices were imaged using an Andor spinning disk (CSU-X1 Yokogawa) confocal system with a 40x 1.15 NA water immersion objective (Nikon) or, for **Fig. S1** and **Fig. S4E**, the Zeiss LSM 710 with 40x 1.1 NA water objective. For pre-ExM confocal imaging, stained slices were treated with an anti-fade buffer (0.05% (w/w) p-phenyldiamine, 20 mM Tris (pH 8.5), 100 mM NaCl). Expanded slices were, for **Figs. 3** and **4**, sandwiched between coverslips of appropriate size (e.g., 45 x 60 mm), forming a chamber which was then backfilled with water and sealed with epoxy. Specimens encapsulated in this way were stable for at least a few days.

Figs. 3E, 3G are maximum intensity projections (MIPs) of 500nm thickness (in pre-ExM distance units), chosen to match the axial extent captured in **Figs. 3D, 3F**, respectively, as closely as possible. **Fig. 3H** is a single z-slice.

For large volume imaging of the mouse hippocampus (**Fig. 4**), the encapsulated expanded specimen was tiled with an array of 12 by 5 z-stacks with ~20% overlap at the boundaries (Nikon). The tiled stacks were downsampled by a factor of 8 for 3D rendering and reconstructed with the ImageJ stitching plugin (*19*). Imaging of these 60 confocal z-stacks, in three colors, with filter switching between each color (required for the low-crosstalk imaging using CMOS cameras in the spinning disk microscope), took ~27 hours.

Optical clearing measurements: Transmission measurements of tissue sections before and after expansion were performed using transmitted white light illumination on a Nikon Ti-E inverted microscope with pass-band filters (480/20, 520/20, 572/20, 610/38) to quantify wavelength dependence, as presented in **Fig S2**. Briefly, 200 μm thick tissue sections were imaged before expansion and after expansion with a 4x 0.13 NA objective with tiling to cover the entire area of the slice. Light transmission was calculated by measuring the transmission intensity of a circular region of interest centered on the tissue slice normalized by the average light transmission absent of the tissue slice.

Post-ExM Residual YFP fluorescence measurements: Unlabeled brain slices (100 μm) from Thy1-YFP-H mice were gelled, digested and expanded as described above, to result in the digestion penetration experiments of **Fig. S1**. Slices were digested with proteinase K for 16 hours. Following digestion, residual YFP fluorescence in cortical pyramidal cells was imaged on a confocal microscope (LSM 710, 40x 1.10 NA water) with pinhole opened to maximum extent (16 Airy units; 16 μm optical sectioning) to collect the dim residual YFP fluorescence. A collection of 25 Z stacks from 2 brain slices were taken across most of the expanded slice thickness (400 μm). To quantify the residual fluorescence at each Z position, the stacks were processed in a custom Matlab script. Briefly, for each image, salt and pepper noise was removed with a [5x5] median filter and the image was segmented into three regions with two thresholds generated via Otsu's method (*20*). The lowest segment of pixel intensities was the background, the middle segment consisted of most of the processes and cell bodies, and the highest segment consisted of a subset of nuclei in which much higher YFP concentrations were present (e.g., see **Fig. 3D** for an example of such a hyper-bright nucleus). The middle segment of pixel intensities

was chosen for the analysis. For each stack, the processed images were averaged for each Z position. The average intensity for each Z position was normalized by the overall average intensity across all Z positions and all stacks for a given brain slice. The normalized average intensity as a function of Z is plotted in **Fig. S1** along with the mean-normalized stack-to-stack standard deviation for each Z position.

Microscopy analysis.

Spinning disk confocal image processing. Standard flatfield correction was performed as needed due to uneven illumination background. Specifically, background was subtracted with a 200 pixel wide 'rolling ball' algorithm as implemented in ImageJ (i.e., **Fig. 2E, 2L, Fig. 4**).

Expansion degree calculation. The expansion degree was determined by choosing two landmarks that could be clearly identified in both pre- and post-expansion images, measuring the distance between these landmarks, and calculating the ratio of this measurement pre- vs. post-expansion. These manually chosen points were used to register the images to each other using a similarity transform (i.e., translation, rotation, and scaling) and the resulting registered images were inspected visually to confirm reasonable registration over the entire specimen.

Non-rigid registration for analysis of measurement errors. Pre- and post-ExM images were first histogram equalized (i.e., for the entire histogram of pixel intensities across each image; Matlab) to each other. Masks were generated to exclude regions with no features by applying a Gaussian blur with a standard deviation of 8 pixels and manually choosing an intensity threshold below which to exclude pixels that were part of the background. (Gaussian blur was used only to generate masks, not for subsequent image processing.) Non-rigid registration between the images was performed using a B-spline-based registration package in Matlab (*21*) using manually selected control points carrying a penalty weight of 1. Registration was performed in four stages with B-spline grids increasing in density from 64 pixels per grid point to 8 pixels per grid point. Analysis of measurement error was performed as schematized in **Fig. S3.**

Microtubule full width at half maximum (FWHM): Intensity profiles perpendicular to microtubule orientation was taken averaging over a line profile width of 10 pixels (~150 nm). Intensity profiles were fit to a Gaussian using the Matlab 'fit' function and the FWHM calculated from the Gaussian fit.

Quantification of clathrin coated pit (CCP) radii: As performed for **Fig. 2O**. Super-resolution structured illumination microscope (SR-SIM) and ExM images of CCPs were first aligned via similarity transform using 2 control points across the field of view. CPPs were identified by visual inspection of ExM z-stacks, and were selected with a rectangular region of interest (ROI, ~2x diameter of pit) so that there were no neighboring pits or background punctate staining within an ROI. For each pit selected in the analysis, its ROI was used to crop the ExM image and corresponding SR-SIM image. A maximum intensity projection of the ExM image corresponding to the same depth of field as the SR-SIM image was chosen to adjust for different optical sectioning thickness, corresponding to ~2 ExM planes (~60 nm/plane in pre-expansion units) for each SR-SIM z-plane (125 nm/plane) chosen. CCP radii were calculated with angular averaging of a radial line profile originating from the centroid of each CCP, with the centroid calculated from the Otsu-binarized image. The angular radial line profile was fit using the Matlab 'fit' function to the sum of 2 Gaussians. The CCP radius was determined to be the half maximum of the fitted angular line profile.

Synapse quantification: Synapses of **Fig. 3** were identified by visual inspection of ExM z-stacks. Candidate instances of closely apposed Bassoon and Homer1 antibody-stained spots were selected from a maximum intensity projection of each stack. Each candidate was then inspected in the original z-stack and selected for inclusion in the analysis if it did not meet any of the following rejection criteria: synapses that were not oriented perpendicular to the imaging plane were recognized when the stained spots shifted continuously between consecutive z-slices, and were rejected; synapses with coincident punctate background staining were rejected; complex assemblies of synapses (e.g., with multiple pre- or post-synaptic terminals) were rejected; synapses that were excessively curved (e.g., relative to the 10-pixel line width, see below) were rejected. For each synapse selected for inclusion in the analysis, a line profile perpendicular to the synaptic cleft was chosen. The staining intensity for Bassoon and Homer1 was analyzed along each line profile, averaging over a width of 10 pixels (~300 nm). The resulting intensity distributions were fit to Gaussian distributions with a DC offset using the Matlab 'fit' function. Any synapses with a resulting goodness of fit, for either Homer1 or Bassoon, of less than 0.9 were rejected. The Bassoon-Homer1 separation was calculated as the separation between the means of the two distributions for each synapse.

Supplementary Figures

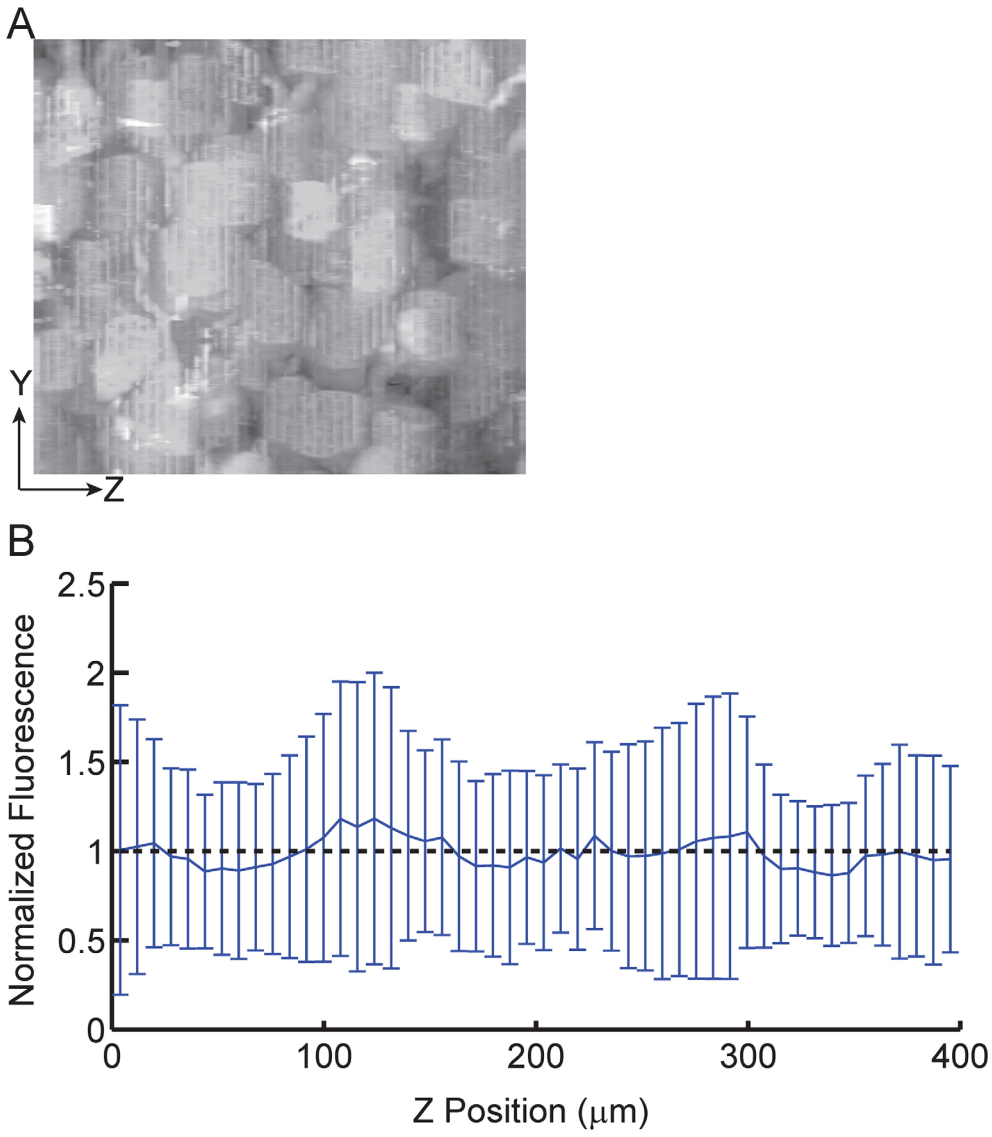

Figure S1. Residual YFP fluorescence as a function of depth in the slice, after digestion and expansion. Proteolysis during the ExM process significantly reduces endogenous YFP fluorescence in expanded samples of Thy1-YFP mouse brain. The residual YFP fluorescence can thus be imaged as a proxy for proteolytic homogeneity. (**A**) Maximum intensity projection in the X dimension of 25 Z stacks of pyramidal cells in the cortex of Thy1-YFP-H brain slices after overnight digestion and subsequent expansion, and processed to exclude high-brightness nuclei and background as described in the **Methods**. The length in the Z dimension is 400 μm in post-expanded units (almost all of the thickness of the 100 μm slice after ~4.5x expansion). (**B**) Mean fluorescence intensity across the stacks of (**A**), normalized by overall mean fluorescence, plotted as a function of Z. Error bars, mean-normalized stack-to-stack standard deviation (n = 25 Z stacks, 2 brain slices). Dotted line, visual reference for fluorescence equal to the mean. The lack of systematic variation of YFP fluorescence vs. depth demonstrates the uniformity of proteolytic digestion throughout the slice.

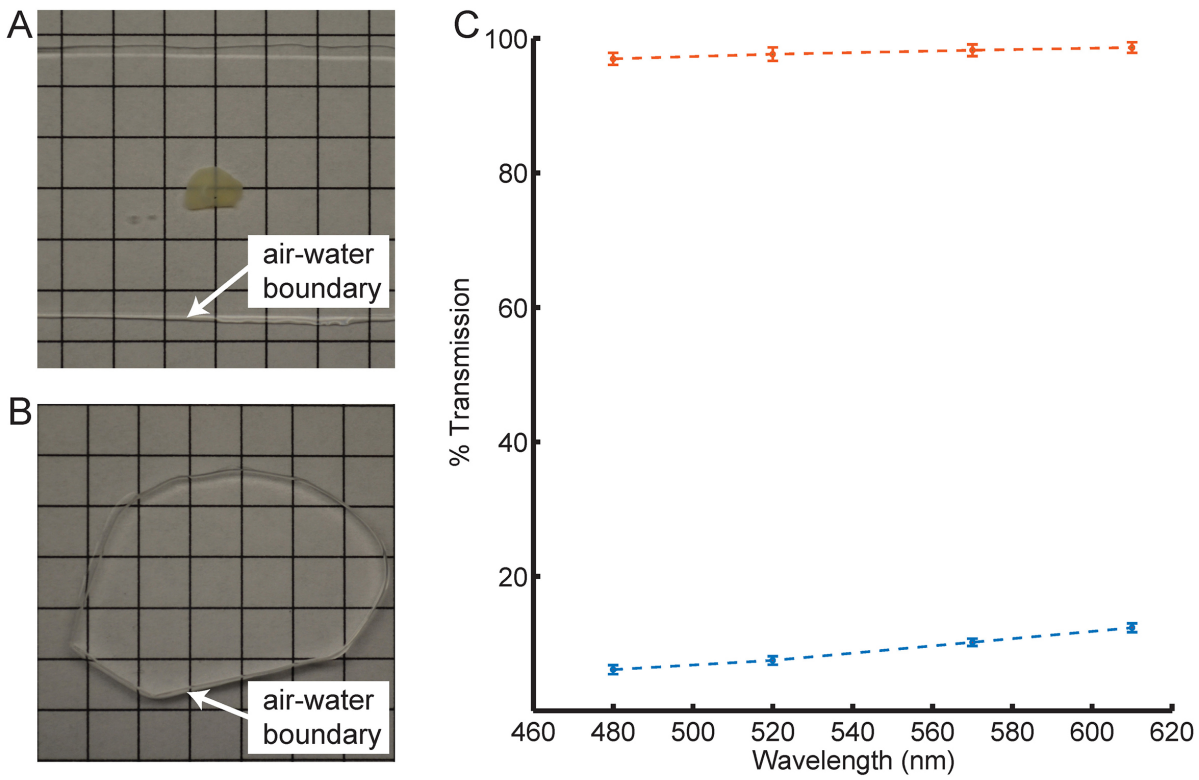

Figure S2. Optical clearing associated with ExM. Expansion significantly reduces scattering of the sample, since the sample is mostly water. A 200 μm fixed brain slice is opaque primarily due to scattering (**A**). However, the post-ExM sample is transparent (**B**). We quantified the transmittance of light through the tissue pre- (blue) vs. post- (orange) ExM processing (**C**).

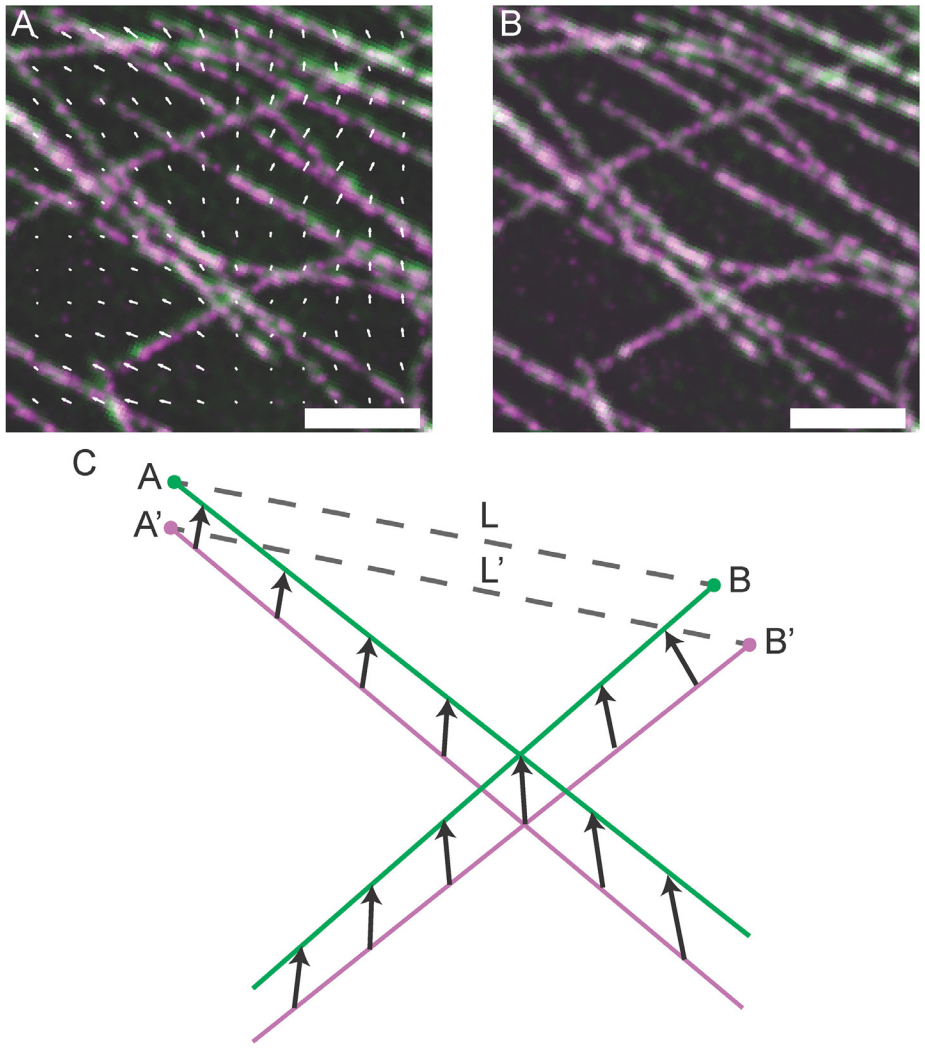

Figure S3. Quantification of Expansion Error Using Non-Rigid Registration. We quantified the error of ExM by deforming the post-ExM image via a non-rigid registration process to attempt an exact match to the pre-ExM image (in contrast to the similarity transform used in **Fig. 2A, 2B** and elsewhere). We used a B-spline based non-rigid registration algorithm (see **Methods**) which generates a vector field that maps the post-ExM image (**A**, magenta) to the pre-ExM image (**A**, green). In (**A**) the overlap between the pre- and post-ExM images appears white, and the deformation vector field (white arrows) is plotted with vector magnitudes scaled by factor of 2 for visibility. The post-ExM image after deformation (**B**, magenta) colocalizes with the pre-ExM image (**B**, green; overlap appears white). Using this deformation field, we can calculate the error of ExM for various length measurements. This is schematized in (**C**): the magenta lines, representing structures in the post-ExM image, are mapped to the green lines, representing the pre-ExM image, via the vector field depicted by black arrows. Measurement L' along the line segment A'B' in the post-ExM image is mapped to measurement L along the line segment AB in the pre-ExM image. The ExM error is calculated as |L-L'|, i.e. the difference between the deformation vectors AA' and BB'. Using the deformation field generated we can calculate the ExM error between all extracted features in the pre- vs. post- images. Scale bars: 1 μm.

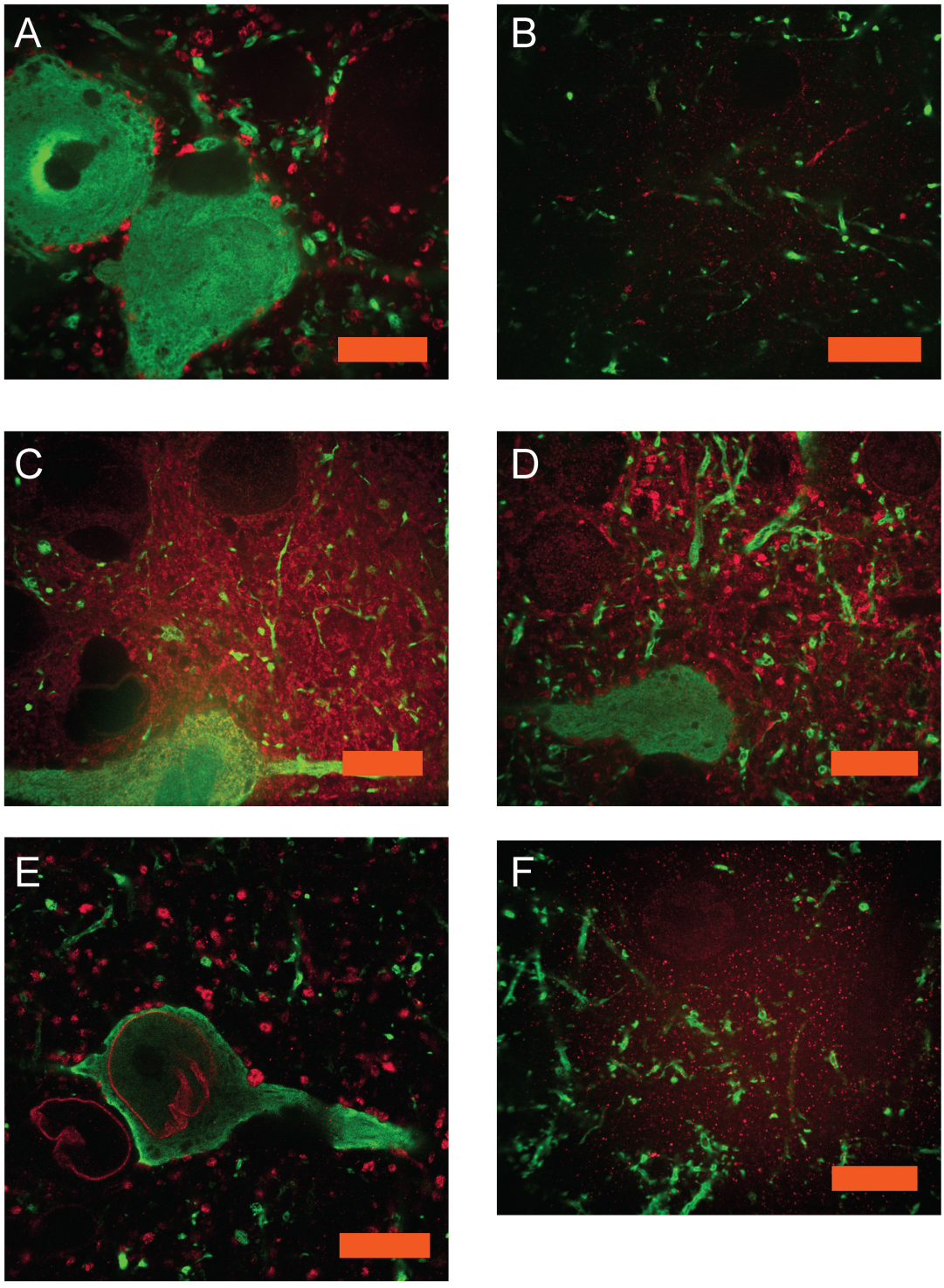

Figure S4. ExM imaging of antibodies of interest in neuroscience and biology. Confocal images of expanded Thy1-YFP mouse brain cerebral cortex sections stained with anti-GFP (green) and antibodies against other proteins (red) as follows: **(A)** GAD65/67 (*22*), **(B)** ChAT (*23*), **(C)** CaMKII (*24*), **(D)** GABA (*25*), **(E)** Lamin A/C (*26*), **(F)** NMDAR2a/b (*27*). Scale bars: **(A)** 10 μm in pre-expansion units (physical size post-expansion, 45 μm); **(B)** 10 μm (47 μm); **(C)** 10 μm (40 μm); **(D)** 10 μm (44 μm); **(E)** 10 μm (43 μm); **(F)** 10 μm (43 μm).

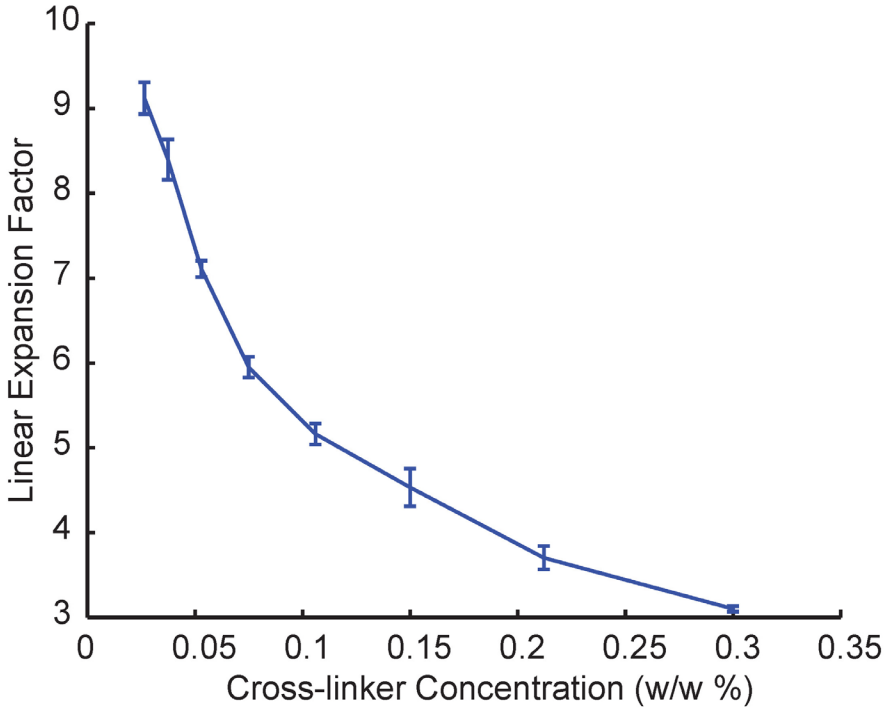

Figure S5. Expansion factor vs. cross-linking. Linear expansion factor for gels cast without specimens, as a function of the concentration of cross-linker used. Error bars represent standard deviation (n = 4 samples).

Supplementary Tables

Table S1. Fluorescence retention during ExM chemical steps.

Fluorescence Retention After Gelation		
	Percent Retention	Standard Deviation (%)
Alexa 488	57.2	2.9 (n = 2 slices)
Atto 565	76.2	0.5 (n = 2 slices)
Atto 647N	58.5	2.8 (n = 2 slices)
Covalent Anchoring Efficiency During Gelation		
	Percentage Anchored	Standard Deviation (%)
Acrydite DNA	87.2	1.1 (n = 4 gels)

Table S2. Chemicals list and suppliers.

	Chemical Name	**Supplier**	**Part Number**
ExM Gel or Preparation	Sodium Acrylate	Sigma	408220
	Acrylamide	Sigma	A9099
	N,N′-Methylenebisacrylamide	Sigma	M7279
	Ammonium Persulfate	Sigma	A3678

	N,N,N′,N′-Tetramethylethylenediamine	Sigma	T7024
	4-Hydroxy-TEMPO	Sigma	176141
Fluorescent Dyes	Alexa 488 NHS ester	Life Technologies	A-20000
	Atto 565 NHS Ester	Sigma	72464
	Atto 647N NHS Ester	Sigma	18373
Hybridization Buffer	Dextran Sulfate	Millipore	S4030
	SSC	Life Tech.	15557
	Yeast tRNA	Roche	10109495001
	Normal Donkey Serum	Jackson Immunoresearch	017-000-001
Fixation and Permeabilization	Paraformaldehyde	Electron Microscopy Sciences	15710
	Glutaraldehyde	Electron Microscopy Sciences	16020
	Triton X-100	Sigma	93426
	Glycine	Sigma	50046
	PBS	Life Technologies	70011-044
Protein Digestion	Proteinase K	New England Biolabs	P8107S
	Ethylenediaminetetraacetic acid	Sigma	EDS
	Guanidine HCl	Sigma	G3272
	Tris-HCl	Life Technologies	AM9855

Table S3. DNA sequences and modifications used for tri-functional labels.

All DNA sequences were ordered from Integrated DNA Technologies, and adapted from (*28*). Each strand for antibody conjugation consists of two 20bp domains separated by two bases of A/T.

Name	Sequence	Modifications
Antibody A	CCGAATACAAAGCATCAACG AA GGTGACAGGGATCACAATCT	5' Amine
Antibody B	TACGCCCTAAGAATCCGAAC TT GCATTACAGTCCTCATAAGT	5' Amine
Antibody C	GACCCTAAGCATACATCGTC TT GACTACTGATAACTGGATTG	5' Amine

Two complementary tri-functional label domains hybridize to each strand conjugated to an antibody. Each antibody strand corresponds to one color of dye.

Name	Sequence	Modifications
A1	CGTTGATGCTTTGTATTCGG	5' Acrydite 3' A488
A2	AGATTGTGATCCCTGTCACC	5' Acrydite 3' A488
B1	GTTCGGATTCTTAGGGCGTA T	5' Acrydite 3' Atto 565
B2	ACTTATGAGGACTGTAATGC T	5' Acrydite 3' Atto 565
C1	GACGATGTATGCTTAGGGTC T	5' Acrydite 3' Atto 647N
C2	CAATCCAGTTATCAGTAGTC T	5' Acrydite 3' Atto 647N

Table S4. Monomer solution recipe.

Component	**Stock concentration***	**Amount (mL)**	**Final concentration***
Sodium acrylate	38	2.25	8.6
Acrylamide	50	0.5	2.5
N,N′-Methylenebisacrylamide	2	0.75	0.15
Sodium chloride	29.2	4	11.7
PBS	10x	1	1x
Water		1	
Total		**9.5****	

*All concentrations in g/100 mL except PBS

This solution is stored as 0.95 mL aliquots, with initiator, accelerator and inhibitor (as needed; see **Methods) added to bring the final volume up to 1 mL per aliquot immediately before each experiment.

Supplementary Movies

Movie S1: 3D animation of large-scale rendering of hippocampal volume from **Fig. 4A**. First, the volume appears with YFP only (green), then staining for Bassoon (blue) and Homer1 (red) are added. Scale bars: 100 μm.

Movie S2: 3D animation of rendered CA1 slm dendrites from **Fig 4B**. Scale bars: 10 μm.

Movie S3: 3D animation of rendered dendritic branch of CA1 slm from **Fig. 4C**, showing YFP (green), Bassoon (blue), and Homer1 (red). Scale bars: 2.5 μm.

Supplementary References

References 19-28 are for the supplementary materials.

References and Notes

1. T. Tanaka, D. Fillmore, S.-T. Sun, I. Nishio, G. Swislow, A. Shah, Phase transitions in ionic gels. *Phys. Rev. Lett.* **45**, 1636–1639 (1980). doi:10.1103/PhysRevLett.45.1636

2. I. Ohmine, Salt effects on the phase transition of ionic gels. *J. Chem. Phys.* **77**, 5725 (1982). doi:10.1063/1.443780

3. F. L. Buchholz, *Superabsorbent Polymers* **573**, 27–38 (1994).

4. B. Huang, S. A. Jones, B. Brandenburg, X. Zhuang, Whole-cell 3D STORM reveals interactions between cellular structures with nanometer-scale resolution. *Nat. Methods* **5**, 1047–1052 (2008). Medline doi:10.1038/nmeth.1274

5. E. H. Rego, L. Shao, J. J. Macklin, L. Winoto, G. A. Johansson, N. Kamps-Hughes, M. W. Davidson, M. G. Gustafsson, Nonlinear structured-illumination microscopy with a photoswitchable protein reveals cellular structures at 50-nm resolution. *Proc. Natl. Acad. Sci. U.S.A.* **109**, E135–E143 (2012). Medline doi:10.1073/pnas.1107547108

6. M. Bates, B. Huang, G. T. Dempsey, X. Zhuang, Multicolor super-resolution imaging with photo-switchable fluorescent probes. *Science* **317**, 1749–1753 (2007). Medline doi:10.1126/science.1146598

7. N. Olivier, D. Keller, P. Gönczy, S. Manley, *PLOS One* **8**, (2013). 10.1371/journal.pone.0069004

8. R. W. Cole, T. Jinadasa, C. M. Brown, Measuring and interpreting point spread functions to determine confocal microscope resolution and ensure quality control. *Nat. Protoc.* **6**, 1929–1941 (2011). Medline doi:10.1038/nprot.2011.407

9. G. Feng, R. H. Mellor, M. Bernstein, C. Keller-Peck, Q. T. Nguyen, M. Wallace, J. M. Nerbonne, J. W. Lichtman, J. R. Sanes, Imaging neuronal subsets in transgenic mice expressing multiple spectral variants of GFP. *Neuron* **28**, 41–51 (2000). Medline doi:10.1016/S0896-6273(00)00084-2

10. A. Dani, B. Huang, J. Bergan, C. Dulac, X. Zhuang, Superresolution imaging of chemical synapses in the brain. *Neuron* **68**, 843–856 (2010). Medline doi:10.1016/j.neuron.2010.11.021

11. A. Rollenhagen, J. H. R. Lübke, The mossy fiber bouton: The “common” or the “unique” synapse? *Front. Synaptic Neurosci.* **2**, 2 (2010). Medline

12. G. R. Newman, B. Jasani, E. D. Williams, A simple post-embedding system for the rapid demonstration of tissue antigens under the electron microscope. *Histochem. J.* **15**, 543–555 (1983). Medline doi:10.1007/BF01954145

13. K. D. Micheva, S. J. Smith, Array tomography: A new tool for imaging the molecular architecture and ultrastructure of neural circuits. *Neuron* **55**, 25–36 (2007). Medline doi:10.1016/j.neuron.2007.06.014

14. B.-C. Chen, W. R. Legant, K. Wang, L. Shao, D. E. Milkie, M. W. Davidson, C. Janetopoulos, X. S. Wu, J. A. Hammer 3rd, Z. Liu, B. P. English, Y. Mimori-Kiyosue, D. P. Romero, A. T. Ritter, J. Lippincott-Schwartz, L. Fritz-Laylin, R. D. Mullins, D. M. Mitchell, J. N. Bembenek, A. C. Reymann, R. Böhme, S. W. Grill, J. T. Wang, G.

Seydoux, U. S. Tulu, D. P. Kiehart, E. Betzig, Lattice light-sheet microscopy: Imaging molecules to embryos at high spatiotemporal resolution. *Science* **346**, 1257998 (2014). Medline doi:10.1126/science.1257998

15. J. Huisken, J. Swoger, F. Del Bene, J. Wittbrodt, E. H. K. Stelzer, Optical sectioning deep inside live embryos by selective plane illumination microscopy. *Science* **305**, 1007–1009 (2004). Medline doi:10.1126/science.1100035

16. J. H. Lee, E. R. Daugharthy, J. Scheiman, R. Kalhor, J. L. Yang, T. C. Ferrante, R. Terry, S. S. Jeanty, C. Li, R. Amamoto, D. T. Peters, B. M. Turczyk, A. H. Marblestone, S. A. Inverso, A. Bernard, P. Mali, X. Rios, J. Aach, G. M. Church, Highly multiplexed subcellular RNA sequencing in situ. *Science* **343**, 1360–1363 (2014). Medline doi:10.1126/science.1250212

17. A. M. Hecht, R. Duplessix, E. Geissler, Structural inhomogeneities in the range 2.5-2500. ANG. in polyacrylamide gels. *Macromolecules* **18**, 2167–2173 (1985). doi:10.1021/ma00153a018

18. D. Calvet, J. Y. Wong, S. Giasson, Rheological monitoring of polyacrylamide gelation: Importance of cross-link density and temperature. *Macromolecules* **37**, 7762–7771 (2004). doi:10.1021/ma049072r

19. S. Preibisch, S. Saalfeld, P. Tomancak, Globally optimal stitching of tiled 3D microscopic image acquisitions. *Bioinformatics* **25**, 1463–1465 (2009). Medline doi:10.1093/bioinformatics/btp184

20. N. Otsu, A threshold selection method from gray-level histograms. *IEEE Trans. Syst. Man Cybern.* **9**, 62–66 (1979). doi:10.1109/TSMC.1979.4310076

21. D.-J. Kroon, "B-spline Grid, Image and Point based Registration"; available at www.mathworks.com/matlabcentral/fileexchange/20057-b-spline-grid--image-and-point-based-registration.

22. C. E. Ribak, Aspinous and sparsely-spinous stellate neurons in the visual cortex of rats contain glutamic acid decarboxylase. *J. Neurocytol.* **7**, 461–478 (1978). Medline doi:10.1007/BF01173991

23. C. R. Houser, G. D. Crawford, P. M. Salvaterra, J. E. Vaughn, Immunocytochemical localization of choline acetyltransferase in rat cerebral cortex: A study of cholinergic neurons and synapses. *J. Comp. Neurol.* **234**, 17–34 (1985). Medline doi:10.1002/cne.902340103

24. B. Tighilet, T. Hashikawa, E. G. Jones, Cell- and lamina-specific expression and activity-dependent regulation of type II calcium/calmodulin-dependent protein kinase isoforms in monkey visual cortex. *J. Neurosci.* **18**, 2129–2146 (1998). Medline

25. S. H. C. Hendry, E. G. Jones, P. C. Emson, D. E. Lawson, C. W. Heizmann, P. Streit, Two classes of cortical GABA neurons defined by differential calcium binding protein immunoreactivities. *Exp. Brain Res.* **76**, 467–472 (1989). Medline doi:10.1007/BF00247904

26. P. Hozák, A. M. Sasseville, Y. Raymond, P. R. Cook, *J. Cell Sci.* **108**, 635–644 (1995).

27. J. M. Fritschy, O. Weinmann, A. Wenzel, D. Benke, Synapse-specific localization of NMDA and $GABA_A$ receptor subunits revealed by antigen-retrieval immunohistochemistry. *J. Comp. Neurol.* **390**, 194–210 (1998). Medline doi:10.1002/(SICI)1096-9861(19980112)390:2<194::AID-CNE3>3.0.CO;2-X

28. H. M. T. Choi, J. Y. Chang, A. Trinh, J. E. Padilla, S. E. Fraser, N. A. Pierce, Programmable in situ amplification for multiplexed imaging of mRNA expression. *Nat. Biotechnol.* **28**, 1208–1212 (2010). Medline doi:10.1038/nbt.1692